Journal of Quantitative Spectroscopy & Radiative Transfer 296 (2023) 108454

Contents lists available at ScienceDirect

Journal of Quantitative Spectroscopy & Radiative Transfer

journal homepage: www.elsevier.com/locate/jqsrt

Controlling the artificial radiance of the night sky: The Añora urban laboratory

Jaime Zamorano[a,b,*], Salvador Bará[c], Manuel Barco[d], Cristóbal García[e], Antonio Luis Caballero[f]

[a] Depto. Física de la Tierra y Astrofísica, Universidad Complutense, Madrid, Spain
[b] Instituto de Física de Partículas y del Cosmos (IPARCOS), UCM, Madrid, Spain
[c] Agrupación Astronómica "Ío", 15005 A Coruña, Galicia, Spain
[d] Agrupación Astronómica de Córdoba, Spain
[e] Asociación Astronómica AstroHenares, Spain
[f] Ayuntamiento de Añora (Córdoba), Spain

ARTICLE INFO

Article history:
Received 28 September 2022
Revised 29 November 2022
Accepted 1 December 2022
Available online 5 December 2022

Keywords:
Light pollution
Radiometry
Photometry
Outdoor lighting

ABSTRACT

We provide radiometric evidence of the relevance of nearby light sources on the artificial brightness of the night sky. To obtain the required data we developed a method based on the use of power-regulated urban lighting systems, which also provides relevant information on the propagation of light pollution at short distances from the sources. A controlled experiment was carried out in the Andalusian municipality of Añora (1526 inhab.) in which the radiant power of its regulated public outdoor lighting system was modified in a predefined way during the central part of the night while continuously recording the zenith sky brightness in the TESS-W photometric band from two separate locations inside the town. We determined that the power-regulated streetlight sources contribute a 60–62% to the total zenith sky brightness at these observing locations in clear and moonless nights when operated at their maximum power rating, being the remaining sky radiance due to constant local sources and sources from neighboring towns. These results, in combination with georeferenced information on the sources' location and properties, impose some constraints on the functional form of the effective point-spread functions (PSF) of the zenith sky brightness at short distances from the sources. For the conditions of our experiment we have found that the expected exponents of power-law PSFs are close to -1.

1. Introduction

Light pollution is a research topic of growing interest. The introduction of anthropogenic light particles in the nighttime environment [11] has been recognized as a form of atmospheric pollution in international treaties [59,60], and its detrimental effects on biodiversity, scientific and cultural heritage, and public health are progressively better known (see e.g. [1,14,15,19,31–33,42,56,57].

One of the most conspicuous manifestations of light pollution is the artificial night sky brightness due to the scattering of artificial light in the terrestrial atmosphere. Although the word 'sky' might suggest to the casual reader that the detected photons are produced only at high altitudes above ground, these scattering events take place along the whole line-of-sight, starting in the very first millimeter from the observer eye or the detector entrance aperture, and comprising all elementary atmospheric volumes illuminated directly or indirectly (after reflections or previous scattering events) by artificial sources. Here we use the word 'brightness' as a convenient shortcut for the in-band radiance, spectrally weighted by the detector passband and angularly averaged over its field of view.

Whereas the propagation of the artificial radiance over distances from a few hundred meters to tens and even hundreds of km from the sources has received considerable attention in the last years, the behavior of the artificial sky brightness at short distances has been much less studied. Anecdotal observation and numerical modeling suggest, however, that the contribution of nearby light sources to the detected sky radiance may be far from negligible in urban settings, where slight displacements of the observer (of order of tens to hundreds of meters) may result in remarkable changes of the brightness of the night sky. Modeling the artificial night sky brightness at medium to long distances from the sources is nowadays accomplished by using different point-spread

* Corresponding author.
E-mail address: jzamorano@fis.ucm.es (J. Zamorano).

https://doi.org/10.1016/j.jqsrt.2022.108454

functions (PSF) that describe the artificial brightness dependence on the source and detector properties, the state of the atmosphere, and the distance to the observer. The interested reader may consult among others the works of Aubé [2], Aubé and Simoneau [3], Bará et al. [4,5,9], Cinzano et al. [16], Cinzano and Falchi [17,18], Duriscoe [20], Falchi et al. [24], Falchi and Bará [26], Garstang [28–30], Kocifaj [35–37], and Simoneau et al. [54] for further details. The basic information about the spatial distribution of the sources and some of their emission properties is available in repositories of nighttime satellite imagery [38–41] as e.g. those of the VIIRS-DNB radiometers onboard the Suomi-NPP and NOAA-20 satellites [21–23, 51,58], the Luojia-01 [34], and the Crew Earth Observation program of the International Space Station [52,53,55].

Most of the PSFs traditionally reported in the literature, however, were not explicitly calculated for distances smaller than a few hundred meters from the source, and scarce experimental data have been collected and reported regarding the behavior of the artificial sky brightness under these circumstances. A theoretical model encompassing all distances from the sources has been recently developed and applied to calculate the expected zenith sky brightness at short and medium distances (see [12], this same special issue).

In the present paper we report observational data gathered in a controlled emissions experiment, in which the night sky brightness was continuously monitored while the emitted radiant flux of the sources was modified in a predefined way. The experiment was carried out on April 2022 in the municipality of Añora, located in Andalusia (Spain), whose public streetlight system was almost fully converted to LED-based luminaires whose emissions can be varied at will from the command center with negligible time constants. This work was made possible through a collaborative action of the technical services of the municipality, who programmed the control sequence of the public lights emissions and set up a measurement sensor, amateur astronomers in charge of another measurement station, and professional scientists in charge of experiment design, data processing, and interpretation. Using already existing power-regulated lighting infrastructures avoids the need of building specific experimental installations and provides a realistic scenario for evaluating city lights emissions. The continued and close collaboration between local authorities, citizen scientists and professional light pollution researchers allows to qualify Añora as an optimum urban lighting laboratory, where high quality data on the effects of public lighting can be acquired in dedicated experiments performed in the central hours of the night across the whole year.

2. Methods

2.1. Ground light emissions and artificial sky brightness

At the usual levels of irradiance of outdoor lighting systems, the artificial sky brightness depends linearly on the emission of the sources. As a particular realization, this means that the artificial zenith spectral radiance $L_\lambda(\mathbf{x}_o)$ measured in the location $\mathbf{x}_o$ at wavelength λ can be written as

$$L_\lambda(\mathbf{x}_o) = \int_S \Psi\left(\mathbf{x}_o,\ \mathbf{x}, \lambda; \boldsymbol{\beta}\right)\ L_s\left(\mathbf{x}; \lambda; \boldsymbol{\beta}_0\right)\ \mathrm{d}^2\mathbf{x}, \tag{1}$$

where $L_s(\mathbf{x};\ \lambda;\ \boldsymbol{\beta}_0)$ is the spectral radiance of the artificial sources located at $\mathbf{x}$ (units $[L_s] = W \cdot \mathrm{m}^{-2} \cdot \mathrm{sr}^{-1} \cdot \mathrm{nm}^{-1}$), $\mathrm{d}^2\mathbf{x}$ is the element of surface in the territory S (units $[\mathrm{d}^2\mathbf{x}] = \mathrm{m}^2$), and $\Psi(\mathbf{x}_o, \mathbf{x},\ \lambda;\ \boldsymbol{\beta})$ is the PSF describing the propagation of light pollution, whose units are in this case $[\Psi] = \mathrm{m}^{-2}$. The units of the PSFs are dependent on the choice of inputs and outputs in the linear system formulation of the light propagation problem. Since in this case the choice for both is a spectral radiance, the PSF units are those that make its product by $\mathrm{d}^2\mathbf{x}$ dimensionless. The symbol $\boldsymbol{\beta} = \{\boldsymbol{\beta}_0, \boldsymbol{\beta}_d, \boldsymbol{\beta}_{atm}\}$ represents a set of several parameter vectors characterizing the properties of source, $\boldsymbol{\beta}_0$ (altitude above ground, angular emission pattern), the observer, $\boldsymbol{\beta}_d$ (altitude above ground, angular sensitivity of the field-of-view of the instrument), and the state of the atmosphere, $\boldsymbol{\beta}_{atm}$ (aerosol concentration profile, optical depth, albedo, asymmetry parameter, etc.), respectively, several of which may also depend on λ.

After an additional integration of $L_\lambda(\mathbf{x}_o)$ over the spectral passband of the detector, $T(\lambda)$, and assuming factorable sources for which the emitted radiance can be expressed as the product of a position-dependent emission amplitude, $L_s(\mathbf{x})$, and a spectral and angular emission term $L_2(\lambda;\ \boldsymbol{\beta}_0)$, that is, $L_s(\mathbf{x};\ \lambda;\ \boldsymbol{\beta}_0) = L_s(\mathbf{x})\, L_2(\lambda;\ \boldsymbol{\beta}_0)$, the detected in-band radiance $L(\mathbf{x}_o)$ can be expressed as a purely spatial integral over the sources' amplitudes:

$$L(\mathbf{x}_o) = \int_S K(\mathbf{x}_o, \mathbf{x})\ L_s(\mathbf{x})\ \mathrm{d}^2\mathbf{x} \tag{2}$$

whose kernel $K(\mathbf{x}_o,\mathbf{x})$, or spatial PSF, is given by:

$$K(\mathbf{x}_o, \mathbf{x}) \equiv \int_\lambda T(\lambda)\ \Psi\left(\mathbf{x}_o,\ \mathbf{x},\ \lambda; \boldsymbol{\beta}\right)\ L_2\left(\lambda; \boldsymbol{\beta}_0\right)\ \mathrm{d}\lambda \tag{3}$$

$K(\mathbf{x}_o,\mathbf{x})$ depends on the parameter set $\boldsymbol{\beta}$, whose symbol is not explicitly indicated but shall be kept in mind. More formal and detailed derivations of these equations, as well as additional discussions on their meaning and range of applicability can be found in Bará and Lima [5], Bará et al. [8,13], and Falchi and Bará [25].

Let us now discretize the sources' territory S in a set of $k = 1, \ldots, N_S$ spatial pixels of area Δ_k (units $[\Delta_k] = \mathrm{m}^2$). The discrete version of Eq. (2) is then:

$$L(\mathbf{x}_o) = \sum_{k=1}^{N_S} K(\mathbf{x}_o, \mathbf{x}_k)\ L_s(\mathbf{x}_k)\ \Delta_k \tag{4}$$

If the sources within each pixel can be controlled in such a way that they may adjust their emitted radiance to a time-dependent fraction $\eta_k(t)$ ($0 \le \eta_k(t) \le 1$) of their maximum emission value $L_s(\mathbf{x}_k)$, the detected artificial radiance in each moment of the night will be:

$$L(\mathbf{x}_o, t) = \sum_{k=1}^{N_S} \eta_k(t)\ K(\mathbf{x}_o, \mathbf{x}_k)\ L_s(\mathbf{x}_k)\ \Delta_k \tag{5}$$

In a controlled urban emissions experiment, a subset of streetlights may typically regulate their power following the same time protocol, $\eta_k(t) \equiv \eta(t)$, $k = 1, \ldots, N_R$, while the remaining ones emit at a constant level $\eta_{k'}(t) \equiv \eta_{k'}$, $k' = 1, \ldots, N_{NR}$, where $N_R + N_{NR} = N_S$. In that case the detected radiance behaves as:

$$L(\mathbf{x}_o,\ t) = \sum_{k'=1}^{N_{NR}} \eta_{k'} K(\mathbf{x}_o, \mathbf{x}_{k'})\ L_s(\mathbf{x}_{k'})\ \Delta_{k'} + \eta(t) \sum_{k=1}^{N_R} K(\mathbf{x}_o, \mathbf{x}_k)\ L_s(\mathbf{x}_k)\ \Delta_k \tag{6}$$

where it has been implicitly assumed that the atmospheric conditions do not change significantly during the experiment, so that the $\boldsymbol{\beta}_k$ parameters are independent of time and so are the PSFs $K(\mathbf{x}_o,\mathbf{x}_k)$. The detected zenith brightness is then the sum of a constant part (due to the not-regulated sources) plus a variable one, dependent on $\eta(t)$.

Equation (6) provides the framework for studying the contribution of a subset of sources to the total sky brightness at a given place, $\mathbf{x}_o$. To achieve this, a controlled experiment can be made in which the sky radiance is measured while the emission fraction $\eta(t)$ is varied following a pre-defined protocol, in time intervals long enough as to allow acquiring sufficient individual measurements in each power emission level to obtain a good signal-to-noise ratio, and short enough as to consider that the remain-

ing sources and the atmospheric conditions do not change significantly during the experiment, something that may be reasonably achieved in the central hours of the night. Denoting by $L(\eta)$ the sky radiance measured as a function of the emission fraction η, by L_0 the sky radiance due of the sources that do not modify their power, and by L_1 the sky radiance due to the sources whose contribution to the total sky brightness we wish to assess, we may rewrite Eq. (6) as

$$L(\eta) = L_0 + \eta L_1 \tag{7}$$

from which the fractional contribution of the regulated sources to the total sky brightness at the observation place $\mathbf{x}_o$ is, for every level of η:

$$f(\eta) = \frac{\eta L_1}{L_0 + \eta L_1} \tag{8}$$

Equation (6) also provides a way of experimentally studying some analytical properties of the spatial PSFs, $K(\mathbf{x}_o,\mathbf{x}_k)$. One of these possibilities is establishing some constraints on the exponents of hypothetical power-laws describing the dependence of $K(\mathbf{x}_o,\mathbf{x})$ on the distance to the sources. If the PSF are shift-invariant and azimuthally symmetric, then $K(\mathbf{x}_o,\mathbf{x}_k) = K(D_{ok})$, where D_{ok} is the horizontal distance between $\mathbf{x}_o$ and $\mathbf{x}_k$, given by the norm of the vector difference $D_{ok} = \|\mathbf{x}_o - \mathbf{x}_k\|$. For a hypothetical power law with exponent α (this exponent is expected to be negative because the PSF should not increase with the distance) the dependence would be $K(D_{ok}) = c_{ok}\ D_{ok}^{\alpha}$, being c_{ok} a constant characteristic of each pixel, dependent on the set of parameters $\boldsymbol{\beta}_k$, which include the spectral and angular emission patterns of the sources and the atmospheric conditions. In this case the slope of $L(\mathbf{x}_o, \eta)$ with respect to η is, according to Eq. (6):

$$\frac{\partial L(\mathbf{x}_o,\ \eta)}{\partial \eta} = \sum_{k=1}^{N_R} c_{0k}\ L_k\ \Delta_k\ D_{ok}^{\alpha} \tag{9}$$

where we use the simplified notation $L_s(\mathbf{x}_k) = L_k$.

In a general case, the values of the constants c_{0k} should be individually determined for each pixel of the territory and moment of the night (if the atmospheric conditions did change). The emission properties of the territory pixels may be different, because of different spectral composition of the sources, spectral reflectance of the neighboring surfaces, source elevations or source angular emission patterns. In the Añora municipality, however, all regulated power sources are LED lamps of essentially equivalent spectra (CCT 3000 K), and with negligible direct emissions to the upper hemisphere so that the most relevant effective source producing the power-regulated part of the artificial sky brightness is the light reflected from the pavements located beneath the streetlights. Assuming the average spectral reflectance of the pixels has the same functional form in the streets of the urban nucleus (the area where the power-regulated streetlights used in our experiment are located), the c_{0k} coefficients can be considered approximately independent from the source and observer locations such that $c_{0k} = c$. Additionally, the area of the pixels used to discretize the territory can be taken uniform, $\Delta_k = \Delta$.

Now, if two detectors A and B are located in different places, the ratio γ of the derivatives with respect to η of the zenith radiances $L(\mathbf{x}_A, \eta)$ and $L(\mathbf{x}_B, \eta)$ measured at both locations is

$$\gamma = \frac{\partial L(\mathbf{x}_A,\ \eta)/\partial \eta}{\partial L(\mathbf{x}_B,\ \eta)/\partial \eta} = \frac{\sum_{k=1}^{N_R} L_k\ D_{Ak}^{\alpha}}{\sum_{k=1}^{N_R} L_k\ D_{Bk}^{\alpha}} \tag{10}$$

where D_{Ak} and D_{Bk} are the distances from the power-regulated source pixels to the detectors and where the constants c and Δ cancel out. Since the values of the radiance L_k emitted from each pixel of the town can be estimated from the radiant power of the lamps, their heights above ground and the ground reflectance, and since the distances to the detectors are known, the modelled value of γ for every exponent α can be directly calculated using Eq. (10). These modeled values can be compared with the ratio γ_{exp} obtained experimentally from measurements of $L(\mathbf{x}_A, \eta)$ and $L(\mathbf{x}_B, \eta)$ as a function of η. This comparison is expected to provide some useful constraints on the compatible values of the power-law exponent α (Section 3.2).

2.2. The Añora public lighting system

Añora (38°24′44″ N, 4°53′51″ W) is a municipality of the autonomous community of Andalusia (Spain), having 1526 inhabitants (2021) and a total extent of 112.57 km^2. It is located in a relatively sparse populated area, at 60 km from the city of Córdoba (322 000 inhab.) and 150 km from Seville (684 000 inhab.). Its public streetlight and outdoor sports lighting system was renewed in the last years by substituting most of the legacy gas-discharge lamps by LED. It is presently composed of 1033 luminaires (Fig 1), of which 737 are fitted with LED lamps of 3000 K correlated color temperature (CCT) and powers ranging from 5 to 118 W, 168 with high pressure sodium vapor (HPS, 70–250 W), 75 with metal halide (MH, 70–400 W), and 53 with fluorescent (FL, 15–30 W) lamps. These luminaires are controlled by eleven independent lighting command panels. While MH and FL lamps operate at a constant luminous flux, most HPS lamps may reduce their emissions in discrete steps to a given fraction of the maximum. All LED lamps can vary their luminous flux in a continuous way, following a programmed protocol, by means of the corresponding command unit.

2.3. TESS-W radiometers

Two STARS4ALL Night Sky Brightness Photometers TESS-W [6,27,45,61], labeled Stars9 and Stars793, are permanently installed in the locations shown in Fig. 1 at 11 and 8 m above ground, respectively, pointing towards the zenith. Their readings can be accessed in real time through the STARS4ALL TESS-W global network website (https://tess.dashboards.stars4all.eu). The TESS-W radiometers are based on an irradiance to RF frequency converter fitted with optics to limit the field of view to an approximately Gaussian region of FWHM 17° Its spectral passband spans the range 400–750 nm. The TESS-W devices provide the sky radiance in units of astronomical magnitudes per square arcsecond, mag$_{TESS}$/arcsec^2. Fig. 2 shows the 'hourglass diagram' of the zenith sky brightness recorded by the radiometer Stars9 in the period 2017–2022.

3. Results

3.1. Dependence of the zenith sky brightness on the artificial light emissions

To investigate the dependence of the zenith sky brightness on the outdoor lighting emissions a dedicated experiment was carried out in Añora, on the night of April 1st to 2nd, 2022 (daylight savings period, official time CEST=UTC+2), under new Moon and with stable and clear atmospheric conditions. The experiment consisted in monitoring the evolution of the zenith sky brightness as the luminous flux emitted by the streetlights varied in a predefined way. A total of 766 luminaires controlled by eight CMA command panels (all panels, excepting CMA-04, CMA-08, and CMA-09) varied synchronously their emissions during the central part of the night according to the protocol shown in the first two columns of Table 1. The corresponding evolution of the raw zenith sky brightness detected by the two TESS-W sensors is shown in Fig. 3, and its mean values (and associated standard deviation of the samples) are listed in columns three to six of Table 1.

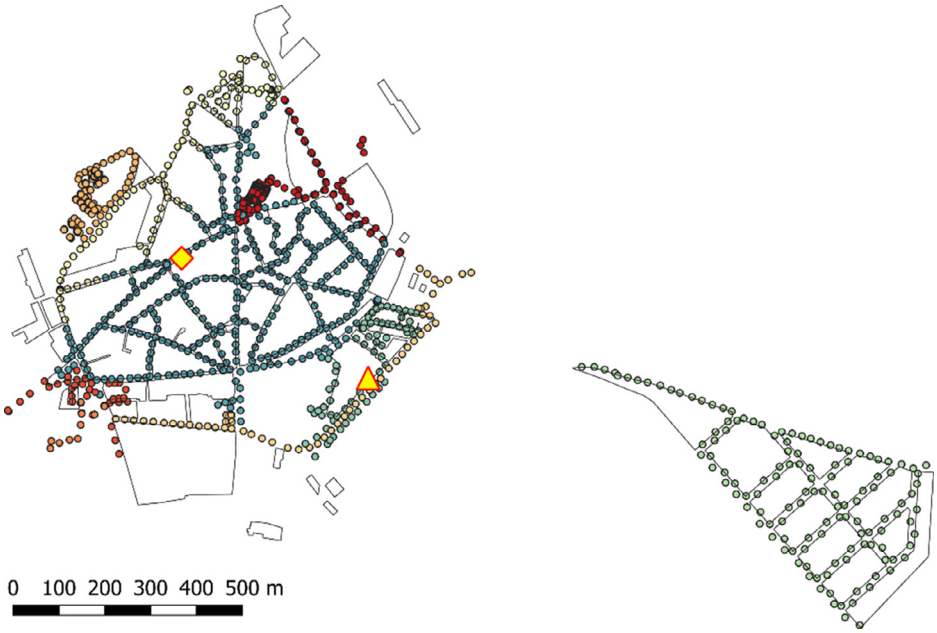

Fig. 1. Layout of the public streetlight system of Añora municipality. Different colors (online) correspond to the sets of luminaires controlled by different command panels. The locations of the detectors TESS-W Stars9 (triangle) and Stars793 (diamond) are also shown.

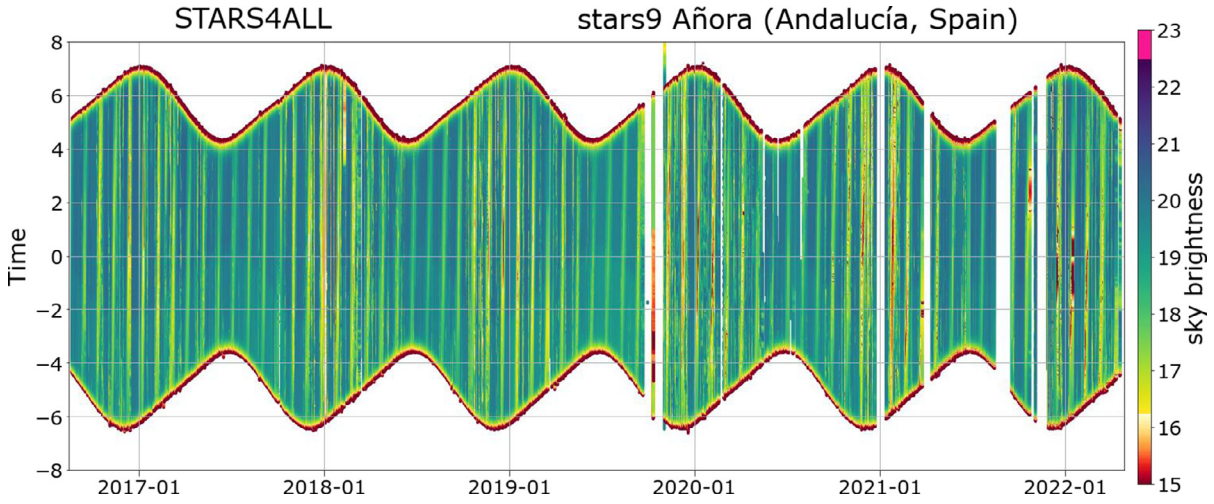

Fig. 2. 'Hourglass diagram' of the zenith sky brightness recorded by the radiometer Stars9 in the town of Añora during the period 2017–2022. Each vertical column corresponds to an individual night. The vertical axis indicates the hour, centered at midnight UTC. The sky brightness is expressed in $\mathrm{mag_{TESS}/arcsec^2}$ using a color scale. White columns represent data not available. The time zone of Añora is UTC+1 (CET), switching to UTC+2 (CEST) during the annual daily savings time period.

Table 1
Synoptic results of the experiment shown in Fig.3. m-values in $\mathrm{mag_{TESS}/arcsec^2}$.

Time (UT)	η	m_{S9} mean	m_{S9} std	m_{S793} mean	m_{S793} std	m^*_{S9} mean
23:00 - 00:00	1.0	20.103	0.0117	20.125	0.0146	19.946
00:30 - 01:00	0.8	20.252	0.0097	20.279	0.0033	20.095
01:00 - 01:30	0.6	20.412	0.0109	20.433	0.0045	20.255
01:30 - 02:00	0.4	20.621	0.0166	20.630	0.0133	20.464
02:00 - 03:00	0.8	20.297	0.0064	20.330	0.0021	20.140

The TESS-W in-band radiance L ($\mathrm{W \cdot m^{-2} \cdot sr^{-1}}$) corresponding to m $\mathrm{mag_{TESS}/arcsec^2}$ is

$$L = C \times 10^{-0.4\ \boldsymbol{m}} \tag{11}$$

where the factor C, with units of radiance, is the radiometric zero-point of the device. It is so called because it defines the zero of the scale of the magnitude system, attained when $L = C$. Eq. (11) is equivalent to

$$m = -2.5\ \log_{10}\left(\frac{L}{C}\right) \tag{12}$$

Whereas the zero-point of a metrological magnitude per square arcsecond scale is unambiguously defined, its practical implementation in different physical sensors may lead to small differences among devices, due to slight variations in the sensor sensitivity, transmittance of the optical components or other unavoid-

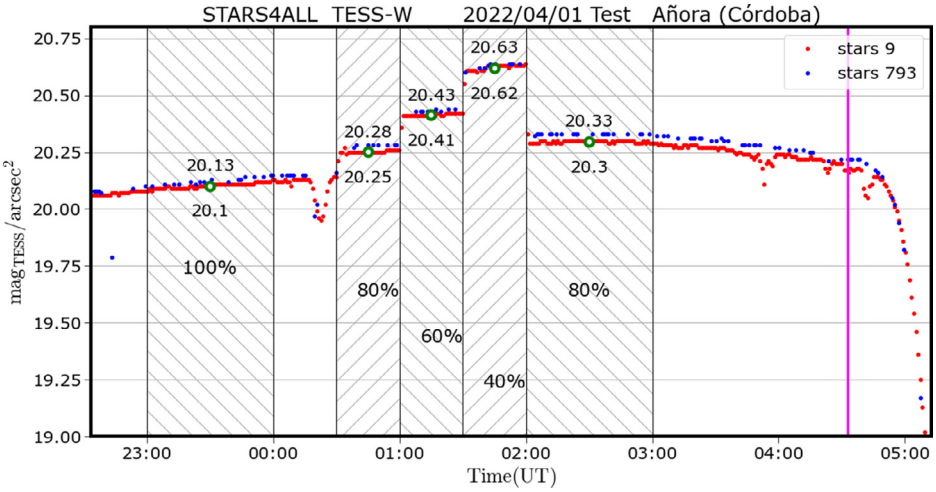

Fig. 3. Time evolution of the raw values of the zenith sky brightness (including the natural and artificial components) recorded by the TESS-W sensors Stars9 and Stars793 in the municipality of Añora, in the night of April 1st to 2nd, 2022. Time in UT, sky brightness expressed in the negative logarithmic scale $\text{mag}_{\text{TESS}}/\text{arcsec}^2$. Values in% indicate the fraction (η) of the maximum power at which the regulated streetlights were operating in each time slot.

able manufacturing factors. Another factor potentially affecting the readings is the different aging of the detectors depending on their cumulative exposure to outdoor conditions, something that has not been reported for the TESS-W units but is known to affect the widely used SQM sensors [10]. In our case, the Stars9 has been installed in its present location since the summer of 2016, whereas the Stars793 was purposely installed for these experiments, having had its "first light" a few days before the measurements here reported were taken. For the science issues addressed in this paper the exact value of the C factors is of little concern, as long as it could be ensured that they are equal for both TESS-W devices. The reason is that the main results we are looking for are related with the percent contribution of the power-regulated streetlight system to the total brightness of the zenith sky, $f(\eta)$ in Eq. (8), as well as with the hypothetical power-law dependence of the light pollution PSFs on the distances from the sources, studied by comparing experimental radiance η-slope ratios against the predicted γ values in Eq. (10). In both calculations the detector constants C_9 and C_{793} cancel out when taking the ratios, provided that $C_9 = C_{793}$.

A calibration procedure must be implemented to ensure that the data provided by both detectors are reported using the same C zero point. In our case the most practical choice was to use the twilight sky as a calibration source, following the clever method developed by Puschnig et al. [50]. This method is based on the fact that, for fixed atmospheric conditions, the twilight zenith sky brightness depends deterministically on the Sun angle below the horizon [46]. Since the sky brightness at the end of the civil twilight and beginning of the nautical one (e.g. with the Sun altitudes in the range −6° to −7°) is considerably higher than the one due to streetlights while it is still within the measurement range of most zenith sky radiance sensors, the twilight sky offers a very useful calibration candle. This calibration can be applied in real time or to historical datasets, without the need of removing the sensors to analyze them in the laboratory. For the usual application of this method, especially if it involves sensors located at distant places, it is advisable to filter out cloudy nights. In our case, however, the procedure is highly simplified due to the fact that both TESS-W units are located a short distance from each other (484 m), such that the natural twilight sky brightness can be considered practically the same at both locations even in cloudy days, excepting perhaps for periods of fragmented clouds or very low altitude cloud layers.

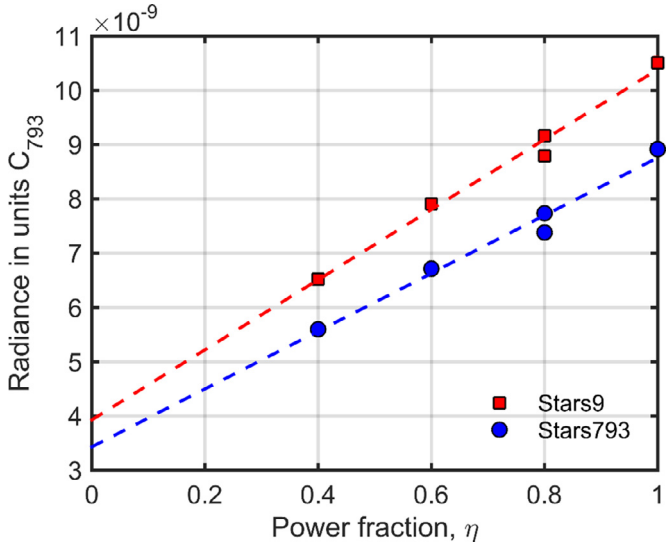

Fig. 4. Radiances of the zenith sky, in units C_{793}, measured by the detectors Stars9 and Stars793 in the experiment shown in Fig. 3., versus the power fraction η at which the regulated streetlights were operating.

For the twilight calibration we selected the data acquired by both sensors when the Sun altitude was in the range [−6°, −7°], in the period from March 30th to June 25th, 2022, resulting in a total of 732 useful records per sensor. Most of the readings at these Sun depression angles were in the range (13.0, 15.5) $\text{mag}_{\text{TESS}}/\text{arcsec}^2$, with only three outliers above the upper limit of this interval. The average bias between the two detectors was found to be $\langle m_{S793} - m_{S9} \rangle_{[-6°,\ -7°]} = -0.157$ (SD: 0.070) $\text{mag}_{\text{TESS}}/\text{arcsec}^2$, where SD is the standard deviation of the data. By applying this correction to the raw readings of detector Stars9 in Table 1 we get the readings referred to the same scale as the Stars793 (column m^*_{S9} mean).

The resulting radiances, in a homogeneous scale with zero-point C_{793} for both detectors, are shown in Fig. 4, as well as their liner regressions fits. The radiances in linear units C_{793} are obtained as $10^{-0.4\,m}$ (Eq. (11)), with m standing for m_{S793} or m^*_{S9}, depending on the detector.

The linear fits of the radiances (in units C_{793}) versus the power fraction η are:

$$L_9(\eta) = 6.455 \times 10^{-9}\ \left(SD: 4.445 \times 10^{-10}\right)\ \eta + 3.929 \times 10^{-9}\ \left(SD:\ 3.326 \times 10^{-10}\right)$$

$$L_{793}(\eta) = 5.327 \times 10^{-9}\ \left(SD: 4.604 \times 10^{-10}\right)\ \eta + 3.432 \times 10^{-9}\ \left(SD:\ 3.445 \times 10^{-10}\right)$$

This means that the fractional contribution of the power-regulated streetlights to the total zenith sky brightness recorded at the central hours of the night at the locations of the detectors, when the sources are operating at maximum power ($\eta = 1$) is, according to Eq. (8) $f_9(1) = 62.2\%$ and $f_{793}(1) = 60.8\%$, respectively. The remaining zenith sky brightness is due to light sources whose emissions did not change significantly during this experiment, including local ones (not-regulated streetlights and other local light sources), streetlights from roadways and neighboring population nuclei and, also, the natural sky, whose contribution to our experiment is significantly lower than that of artificial light [43,44].

The ratio of the experimental derivatives with respect to η, which is of interest for studying the hypotetical power-law of the propagation of light pollution at short distances from the sources, see Eq.(10) and next subsection, is then

$$\gamma_{exp} = \frac{dL_{793}(\eta)/d\eta}{dL_9(\eta)/d\eta} = 0.825\ \ (SD: 0.091) \tag{13}$$

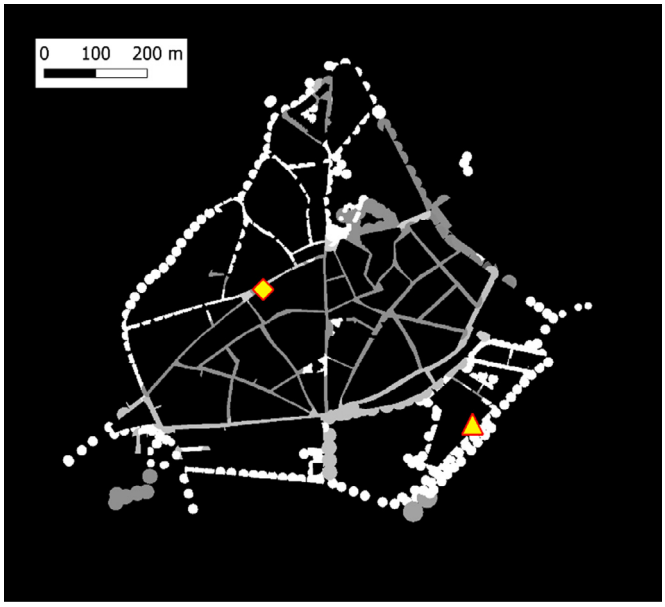

Fig. 5. Illustrating the estimated relative street irradiance produced by the power-regulated luminaires in Añora town, from the data available in the municipality lighting inventory. The locations of the detectors Star9 (triangle) and Stars793 (diamond) are also shown.

3.2. Constraining the exponents of PSF power-laws

The data gathered in this experiment permit to obtain some preliminary insights about the power-law dependence of the zenith sky brightness on the distance to the sources, in the short- to mid-distances range. To that end we can compare the ratio γ_{exp} obtained experimentally, Eq. (13), with the γ that could be expected from different exponents α in the power-law model Eq. (10). For applying Eq.(10) we shall carry out a summation over the source radiances, L_k, weighted by the α-powers of the distances to the detectors. It shall be kept in mind that the detectors are installed on building roofs, above the street level, and that the air column above them is not directly illuminated by the street lamps, but rather by the light reflected from the pavements (and, up to a certain height, from the buildings façades). Each small portion of the streets (pixel k), illuminated by the lamp(s) above it with an irradiance E_k [W · m^{-2}] can be considered as an approximate Lambertian emitter, whose radiance is $L_k = (\rho_k/\pi)E_k$ [W · m^{-2} · sr^{-1}], where ρ_k is the reflectance of the ground.

Since a high-resolution map of the actual radiances of the street pixels L_k is still not available, an approximate estimation of these radiances can be made using the municipality lighting inventory, which contains, among other information, the precise location, type, power and height above ground of each streetlight in the town. Since we are only interested in the radiance due to the power-regulated sources (recall that Eq.(10) applies to the ratio of the derivatives of the radiance L_k vs η), an estimate of the street radiance can be made by dividing the city raster map in small square pixels of side 0.5 m (area $\Delta = 0.25$ m^2), and assigning to each pixel an average irradiance proportional to the electric power of the nearest lamp divided by the area of the street illuminated by that lamp. Using the electrical power as a proxy for the lamp radiant flux is justified in this experiment, since it involves a very homogeneous set of lamps (LED 3000 K) with essentially uniform luminous efficacy. The area illuminated by each streetlight can be approximated by a circle of radius $r_k = n\, h_k$, where h_k is the height of the lamp pole illuminating the pixel k, and n is the ratio of the average semi-distance of the luminaires to their heights, here taken as $n = 2.5$. The irradiance on the pixel k is then $E_k = P_k/[\pi(nh_k)^2]$ and the reflected radiance is $L_k = \rho_k P_k/(\pi n h_k)^2$. Under the admittedly oversimplifying assumption of uniform reflectance across the town streets, $\rho_k = \rho$, the pixel radiances become proportional to $P_k/(nh_k)^2$. Fig. 5 depicts the relative street irradiance produced by the power-regulated lamps. It applies to any η level ($0 < \eta \leq 1$) since all regulated lamps used in our experiment synchronously varied their power following the same protocol.

With the estimated values of the radiances L_k ($k = 1, \ldots, N_R$) and the horizontal distances from the ground pixels to the detectors D_{Ak} and D_{Bk}, where A stands for the Stars793 and B for the Stars9, the ratio $\gamma(\alpha)$ between the expected slopes of the radiance vs η can be calculated using Eq.(10) for the hypothetical case of a power law with exponent α. Recall that any constant factor affecting the estimation of the L_k cancels out when taking the ratio, so the values of $P_k/(nh_k)^2$ can be used instead of L_k as long as our assumption about the uniform pixel reflectance holds. Fig. 6 shows the results of this calculation, for the positions of our detectors and for values of the power-law exponent $-2 \leq \alpha \leq 0$.

Estimations for three different values of the ratio semi-distance/heigh of the lamposts ($n = 2.0$, 2.5 and 3.0) are shown in this Figure, to get some insights about the dependence of the results on this parameter. Although for a fixed set of pixels this parameter cancels out in the numerator and denominator of the ratio, some differences may be expected if n is changed. The reason is that since the pixel size used in this calculation was very small, $\Delta = 0.25$ m^2, for adequately representing the illuminated areas near the locations of the detectors (the ratio of power laws is very sensitive to the radiances at very short distances D_{Ak} and D_{Bk}), the number of pixels effectively illuminated in certain zones of the map may change depending on the radius of the illuminated zone beneath each lamp, which in turn depends on n. So N_R in Eq. (19) may depend on the choice of n. The observational value of γ_{exp}, Eq.(13), obtained in our experiment is shown as an horizontal line with intervals of one standard deviation above and below. It can be seen that our experimental result is reasonably compatible with power laws of exponent $\alpha \in [-1.45,\ -0.85]$, if the interval

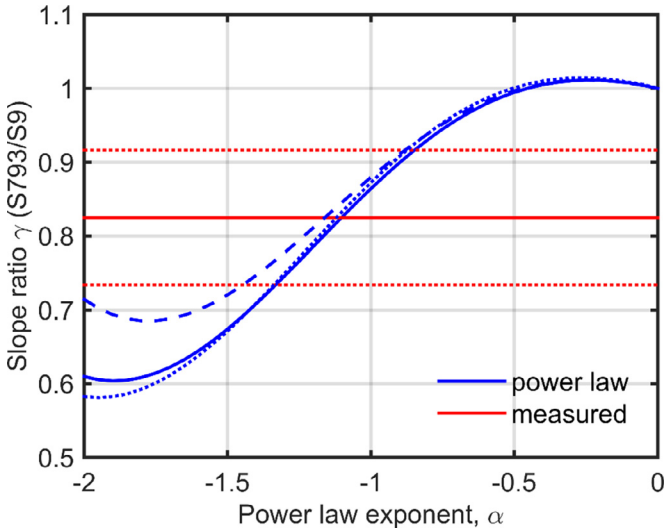

Fig. 6. (Color online) *Blue*: Slope ratio $\gamma(\alpha)$ estimated from the Añora pixel radiances using the power law in Eq. (10) for the locations of the detectors Stars793 and Stars9, with $n=2.5$ (full line), $n=2.0$ (dashed line) and $n=3.0$ (dotted line). *Red*: measured value γ_{exp}, Eq. (13) (full line) and intervals of one standard deviation (dotted lines).

of one standard deviation of γ_{exp} is taken as a measure of compatibility. Note however that no sharp conclusions should be taken from this result, since the number of experimental data used to calculate γ_{exp} is small and so are the degrees of freedom. Adopting a reasonable degree of confidence (e.g. 95%) would lead to very large confidence intervals which would not allow excluding a much broader range of exponents. This result is, nevertheless, a reasonable indication that the zenith sky brightness may depend on the distance as a power law with exponent close to −1 for observers located up to several hundred meters from the sources.

4. Discussion

This work highlights the usefulness of power-regulated outdoor lighting systems for obtaining relevant information on the propagation of the artificial brightness of the night sky. By monitoring the evolution of the sky radiance while the luminaire emissions are changed in a controlled way it is possible to estimate the contribution of these luminaires to the total sky brightness as well as to put some constraints on the exponents of the power-laws that may describe the propagation of light pollution at short to mid-distances from the sources.

We have found that our measurements are compatible with a power-law dependence of the artificial zenith sky brightness on the distance to the sources, with exponent close to −1. The choice of a constant exponent power-law as a trial function is justified by the small range of distances involved in our experiment (no larger than $\sim$ 1 km). It is well-known from the scientific literature that the theoretical log-log curves of PSFs vs distance over long distance ranges (up to hundreds of km) have a variable slope, which tends to become more negative with distance. A single constant exponent is then expected to characterize this behavior only over a limited distance range, as it was our case. The exponent we found is consistent with the one expected from numerical calculations with models like Illumina v2 for this range of distances, see e.g. Simoneau et al. [54], and it is also consistent with the exponent −1 expected from short-distance analytical approximations to the scattering integrals [12]. Further field studies should try to reduce even more the uncertainty of the experimental estimates of this exponent, to validate the predictions of different theoretical models taking into account the small-scale details of the lighting installations.

The results presented in this paper are contingent on several main assumptions and are affected by some experimental limitations. One is the assumption of factorability of the spatial and angular-spectral terms of the sources' radiance used to deduce Eq.(2). Other is the assumption of equality of the c_{0k} coefficients that allows writing the γ ratio in the simplified form shown in Eq. (10). The assumption that the coefficient c_{0k} multiplying the power-law factor of the PSF is the same for all source pixels is valid as long as the parameters contained in the vector set $\boldsymbol{\beta}_k$, which include the spectral and angular emission patterns of the sources and the atmospheric conditions, are equal for these pixels. The quantitative computation of the expected $\gamma(\alpha)$ in Añora for several exponents (Section 3.2) has been made from an approximate estimation of the street irradiances based on the municipal lighting inventory. A more precise treatment could be made by using actual street radiance data, obtained by means of satellite or airborne nocturnal imaging. Another experimental limitation regards the twilight calibration, typically performed under zenith sky brightness in the range 13.0–15.5 $\mathrm{mag_{TESS}/arcsec^2}$. Although the linearity of the detectors reasonably permits to apply the inter-device zero-point calibration factor obtained in these conditions to the typical brightnesses recorded in the experiment, close to 20.0–20.5 $\mathrm{mag_{TESS}/arcsec^2}$, the different angular distribution of the sky brightness patterns of the natural twilight and the artificial lights could lead to some uncompensated error, if a slight relative misalignment of the centers of the detectors' fields of view were present in the experiment.

Not as a limitation of this experiment, but as a general comment, the percent contribution of a subset of lamps to the total brightness of the night sky depends on the relative location of the lamps and the observer, the time evolution of the remaining artificial emissions, and the state of the atmosphere. The latter may significantly vary in timescales from minutes to seasons. This underscores the fact that the sky brightness is not a fixed number but a variable quantity that should be statistically handled to derive averaged indicators for each site, relatively stable from year to year excepting for variations of the anthropogenic emissions or inter-annual trends in local climate conditions, see e.g. Puschnig et al. [48,49], Posch et al. [47], Bará et al. [7]. The percent contributions $f_9(\eta=1)=62.2\%$ and $f_{793}(\eta=1)=60.8\%$, obtained in Section 3.1 shall then be understood as particular realizations of these variables.

Conclusions

Power-regulated emissions from public outdoor lighting systems offer an interesting opportunity for studying relevant aspects of the propagation of the artificial night sky brightness. Leveraging on the existing public lighting installations to perform the experiments avoids the need of building additional expensive and environmentally unfriendly outdoor testing grounds. The possibility of synchronously switching the amount of luminous flux emitted by part or the whole streetlight system provides an easy way for isolating its relative contribution to the total effects, by analyzing its time signature in the recorded brightness. With modern solid-state light sources and control panels the changes in the luminous flux can be exceedingly fast in time, only limited in practice by the number of measurements that have to be made in each constant power step in order to achieve a sufficient signal to noise ratio. In this study we have found that the contribution of the power-regulated streetlights to the total sky brightness in the town of Añora is of order 60–62%, at the locations of our detectors. We have also estimated experimentally that the exponent of a power-law describing the dependence of the zenith sky brightness on the

distance to the sources, at short distances from them, should fall within the range [– 1.45, – 0.85]. This is compatible with theoretical predictions that estimate this exponent to be equal to –1. The results presented in this paper also highlight the strong synergies achievable by joint collaboration of academic researchers, public authorities and citizen scientists.

Declaration of Competing Interest

The authors declare that they have no known competing financial interests or personal relationships that could have appeared to influence the work reported in this paper.

Data Availability

Data will be made available on request.

Acknowledgments

The authors acknowledge the full collaboration of the public authorities of Añora, and the useful suggestions of two anonymous reviewers for improving the first version of this manuscript.

Funding sources

Jaime Zamorano is funded by Ministerio de Ciencia Innovación, Plan Estatal de Investigación Científica, Técnica y de Innovación 2021-2023 (PID2021-123417OB-I00).

References

[1] American Medical Association (AMA), 2012. Light Pollution: adverse health effects of nighttime lighting, in: Proceedings of the American Medical Association House of Delegates, 161st annual meeting, Chicago, Illinois (USA) pp 265–79 (2012). Online: https://www.ama-assn.org/sites/ama-assn.org/files/corp/media-browser/public/hod/a12-csaph-reports_0.pdf
[2] Aubé M. Light pollution modelling and detection in a heterogeneous environment. In: Marín C, Jafari J, editors. StarLight: a common heritage; starlight initiative la Palma biosphere reserve, instituto de astrofísica de canarias, government of the canary islands. Spain: Spanish Ministry of The Environment, UNESCO-MaB: Canary Islands; 2008. p. 351–8.
[3] Aubé M, Simoneau A. New features to the night sky radiance model illumina: hyperspectral support, improved obstacles and cloud reflection. J Quant Spectrosc Radiat Transfer 2018;211:25–34. doi:10.1016/j.jqsrt.2018.02.033.
[4] Bará S, Ribas SJ, Kocifaj M. Modal evaluation of the anthropogenic night sky brightness at arbitrary distances from a light source. J Opt 2015;17:105607. doi:10.1088/2040-8978/17/10/105607.
[5] Bará S, Lima RC. Photons without borders: quantifying light pollution transfer between territories. Int J Sustain Lighting 2018;20(2):51–61. doi:10.26607/ijsl.v20i2.87.
[6] Bará S, Tapia CE, Zamorano J. Absolute radiometric calibration of TESS-W and SQM night sky brightness sensors. Sensors 2019;19(6):1336. doi:10.3390/s19061336.
[7] Bará S, Lima RC, Zamorano J. Monitoring long-term trends in the anthropogenic brightness of the night sky. Sustainability 2019;11:3070 b. doi:10.3390/su11113070.
[8] Bará S, Falchi F, Furgoni R, Lima RC. Fast Fourier-transform calculation of artificial night sky brightness maps. J Quant Spectrosc Radiat Transf 2020;240:106658. doi:10.1016/j.jqsrt.2019.106658.
[9] Bará S, Falchi F, Lima RC, Pawley M. Can we illuminate our cities and (still) see the stars? Int J Sustain Lighting IJSL 2021;23(2):58–69. doi:10.26607/ijsl.v23i2.113.
[10] Bará S, Marco E, Ribas SJ, Garcia-Gil M, Sánchez de Miguel A, Zamorano J. Direct assessment of the sensitivity drift of SQM sensors installed outdoors. Int J Sustain Lighting 2021;23:1–6 b. doi:10.26607/ijsl.v23i1.109.
[11] Bará S, Bao-Varela C, Falchi F. Light pollution and the concentration of anthropogenic photons in the terrestrial atmosphere. Atmos Pollut Res 2022;13(9):101541 a. doi:10.1016/j.apr.2022.101541.
[12] Bará S., Bao-Varela C., Kocifaj M. 2022b. Modelling the artificial night sky brightness at short distances from streetlights. J Quant Spectrosc Radiat Transf (in press).
[13] Bará S, Pérez-Couto X, Falchi F, Kocifaj M, Masana E. Estimating linear radiance indicators from the zenith night-sky brightness: on the Posch ratio for natural and light-polluted skies. Mon Not R Astron Soc 2022;512(2):2125–34 c. doi:10.1093/mnras/stac410.
[14] Bonmati-Carrion MA, Arguelles-Prieto R, Martinez-Madrid MJ, Reiter R, Hardeland R, Rol MA, Madrid JA. Protecting the melatonin rhythm through circadian healthy light exposure. Int J Mol Sci 2014;15:23448–500. doi:10.3390/ijms151223448.
[15] Brown TM, Brainard GC, Cajochen C, Czeisler CA, Hanifin JP, Lockley SW, et al. Recommendations for daytime, evening, and nighttime indoor light exposure to best support physiology, sleep, and wakefulness in healthy adults. PLoS Biol 2022;20(3):e3001571. doi:10.1371/journal.pbio.3001571.
[16] Cinzano P, Falchi F, Elvidge C. The first world atlas of the artificial night sky brightness. Mon Not R Astron Soc 2001;328:689–707. doi:10.1046/j.1365-8711.2001.04882.x.
[17] Cinzano P, Falchi F. The propagation of light pollution in the atmosphere. Mon Not R Astron Soc 2012;427:3337–57. doi:10.1111/j.1365-2966.2012.21884.x.
[18] Cinzano P, Falchi F. Quantifying light pollution. J Quant Spectrosc Radiat Transfer 2014;139:13–20. doi:10.1016/j.jqsrt.2013.11.020.
[19] Davies TW, Bennie J, Inger R, Gaston KJ. Artificial light alters natural regimes of night-time sky brightness. Sci Rep 2013;3:1722. doi:10.1038/srep01722.
[20] Duriscoe DM, Anderson SJ, Luginbuhl CB, Baugh KE. A simplified model of all-sky artificial sky glow derived from VIIRS Day/Night band data. J Quant Spectrosc Radiat Transf 2018;214:133–45. doi:10.1016/j.jqsrt.2018.04.028.
[21] Elvidge CD, Baugh K, Zhizhin M, Hsu FC, Ghosh T. VIIRS night-time lights. Int J Rem Sens 2017;38(21):5860–79. doi:10.1080/01431161.2017.1342050.
[22] Elvidge CD, Zhizhin M, Ghosh T, Hsu F-C, Taneja J. Annual time series of global VIIRS nighttime lights derived from monthly averages: 2012 to 2019. Remote Sens 2021;13:922. doi:10.3390/rs13050922.
[23] Elvidge CD, Baugh K, Ghosh T, Zhizhin M, Hsu FC, Sparks T, Bazilian M, Sutton PC, Houngbedji K, Goldblatt R. Fifty years of nightly global low-light imaging satellite observations. Front Rem Sens 2022;3:919937. doi:10.3389/frsen.2022.919937.
[24] Falchi F, Cinzano P, Duriscoe D, Kyba CCM, Elvidge CD, Baugh K, Portnov BA, Rybnikova NA, Furgoni R. The new world atlas of artificial night sky brightness. Sci Adv 2016;2:e1600377. doi:10.1126/sciadv.1600377.
[25] Falchi F, Bará S. A linear systems approach to protect the night sky: implications for current and future regulations. R.Soc. Open Sci. 2020;7:201501. doi:10.1098/rsos.201501.
[26] Falchi F, Bará S. Computing light pollution indicators for environmental assessment. Nat Sci 2021:e10019. doi:10.1002/ntls.10019.
[27] García L., Zamorano J., Tapia C. 2018, Tess photometer manual. doi: 10.5281/zenodo.1492285.
[28] Garstang RH. Model for artificial night-sky illumination. Publ Astron Soc Pac 1986;98:364–75.
[29] Garstang RH. Night-sky brightness at observatories and sites. Publ Astron Soc Pac 1989;101:306–29.
[30] Garstang RH. Dust and light pollution. Publ Astron Soc Pac 1991;103:1109–16.
[31] Gaston KJ, Ackermann S, Bennie J, Cox DTC, Phillips BB, Sánchez de Miguel A, Sanders D. Pervasiveness of biological impacts of artificial light at night. Integr Comp Biol 2021;61(3):1098–110. doi:10.1093/icb/icab145.
[32] Hölker F, Wolter C, Perkin EK, Tockner K. Light pollution as a biodiversity threat. Trends Ecol Evolut 2010;25(12):681–2. doi:10.1016/j.tree.2010.09.007.
[33] Hölker F, Bolliger J, Davies TW, Giavi S, Jechow A, Kalinkat G, Longcore T, Spoelstra K, Tidau S, Visser ME, Knop E. 11 Pressing research questions on how light pollution affects biodiversity. Front Ecol Evol 2021;9:767177. doi:10.3389/fevo.2021.767177.
[34] Jiang W, He G, Long T, Guo H, Yin R, Leng W, Liu H, Wang G. Potentiality of using Luojia 1-01 nighttime light imagery to investigate artificial light pollution. Sensors 2018;18:2900. doi:10.3390/s18092900.
[35] Kocifaj M. Light-pollution model for cloudy and cloudless night skies with ground-based light sources. Appl Opt 2007;46:3013–22.
[36] Kocifaj M. A review of the theoretical and numerical approaches to modeling skyglow: iterative approach to RTE, MSOS, and two-stream approximation. J Quant Spectrosc Radiat Transf 2016;181:2–10.
[37] Kocifaj M. Multiple scattering contribution to the diffuse light of a night sky: a model which embraces all orders of scattering. J Quant Spectrosc Radiat Transfer 2018;206:260–72. doi:10.1016/j.jqsrt.2017.11.020.
[38] Kyba CCM, Garz S, Kuechly H, Sánchez de Miguel A, Zamorano J, Fischer J, Hölker F. High-resolution imagery of earth at night: new sources, opportunities and challenges. Remote Sens 2015;7:1–23. doi:10.3390/rs70100001.
[39] Levin N, Kyba CCM, Zhang Q. Remote sensing of night lights—beyond DMSP. Remote Sens 2019;11:1472. doi:10.3390/rs11121472.
[40] Levin N, Kyba CCM, Zhang Q, Sánchez de Miguel A, Román MO, Li X, Portnov BA, Molthan AL, Jechow A, Miller SD, Wang Z, Shrestha RM, Elvidge CD. Remote sensing of night lights: a review and an outlook for the future. Remote Sens Environ 2020;237:111443. doi:10.1016/j.rse.2019.111443.
[41] Li X, Elvidge C, Zhou Y, Cao C, Warner T. Remote sensing of night-time light. Int J Rem Sens 2017;38(21):5855–9. doi:10.1080/01431161.2017.1351784.
[42] Marín C, Jafari J. StarLight: a common heritage; starlight initiative la Palma biosphere reserve, instituto de astrofísica de Canarias, government of the canary islands. Spain: Spanish Ministry of The Environment, UNESCO-MaB: Canary Islands; 2008.
[43] Masana E, Carrasco JM, Bará S, Ribas SJ. A multi-band map of the natural night sky brightness including Gaia and Hipparcos integrated starlight. Mon Not R Astron Soc 2021;501:5443–56. doi:10.1093/mnras/staa4005.
[44] Masana E, Bará S, Carrasco JM, Ribas SJ. An enhanced version of the Gaia map of the brightness of the natural sky. Int J Sustain Lighting 2022;24(1):1–12. doi:10.26607/ijsl.v24i1.119.
[45] Pascual S., Zamorano J., González E., Tapia C., González R., García C., García L., Sánchez-Penim A., et al. Citizen science with the TESS photometer network. Astronomical data analysis software and systems XXX, ASP conference series 2021;532. J. E. Ruiz, F. Pierfederici, and P. Teuben, editors 2021 Astronomical Society of the Pacific

[46] Patat F, Ugolnikov OS, Postylyakov OV. UBVRI twilight sky brightness at ESO-Paranal. Astron Astrophys 2006;455:385–93. doi:10.1051/0004-6361:20064992.
[47] Posch T, Binder F, Puschnig J. Systematic measurements of the night sky brightness at 26 locations in Eastern Austria. J Quant Spectrosc Radiat Transf 2018;211:144–65. doi:10.1016/j.jqsrt.2018.03.010.
[48] Puschnig J, Posch T, Uttenthaler S. Night sky photometry and spectroscopy performed at the Vienna University Observatory. J Quant Spectrosc Radiat Transf 2014;139:64–75.
[49] Puschnig J, Schwope A, Posch T, Schwarz R. The night sky brightness at Potsdam-Babelsberg including overcast and moonlit conditions. J Quant Spectrosc Radiat Transf 2014;139:76–81.
[50] Puschnig J, Näslund M, Schwope A, Wallner S. Correcting sky-quality-meter measurements for ageing effects using twilight as calibrator. Mon Not R Astron Soc 2021;502:1095–103. doi:10.1093/mnras/staa4019.
[51] Román MO, Wang Z, Sun Q, Kalb V, Miller SD, Molthan A, Schultz L, Bell J, et al. NASA's Black Marble nighttime lights product suite. Remote Sens Environ 2018;210:113–43. doi:10.1016/j.rse.2018.03.017.
[52] Sánchez de Miguel A, Kyba CCM, Aubé M, Zamorano J, Cardiel N, Tapia C, Bennie J, Gaston KJ. Colour remote sensing of the impact of artificial light at night (I): the potential of the International Space Station and other DSLR-based platforms. Remote Sens Environ 2019;224:92–103. doi:10.1016/j.rse.2019.01.035.
[53] Sánchez de Miguel A, Zamorano J, Aubé M, Bennie J, Gallego J, Ocaña F, Pettit DR, Stefanov WL, Gaston KJ. Colour remote sensing of the impact of artificial light at night (II): calibration of DSLR-based images from the International Space Station. Rem Sens Environ 2021:112611. doi:10.1016/j.rse.2021.112611.
[54] Simoneau A, Aubé M, Leblanc J, Boucher R, Roby J, Lacharité F. Point spread functions for mapping artificial night sky luminance over large territories. Mon Not R Astron Soc 2021;504(1):951–63. doi:10.1093/mnras/stab681.
[55] Stefanov WL, Evans CA, Runco SK, Wilkinson MJ, Higgins MD, Willis K, et al. Astronaut photography: handheld camera imagery from low earth orbit Handbook of satellite applications. Pelton JN, et al., editors. Springer International Publishing Switzerland; 2017. doi:10.1007/978-3-319-23386-4_39.
[56] Stevens RG, Brainard GC, Blask DE, Lockley SW, Motta ME. Breast cancer and circadian disruption from electric lighting in the modern world. CA Cancer J Clin 2014;64:207–18. doi:10.3322/caac.21218.
[57] Svechkina A, Portnov BA, Trop T. The impact of artificial light at night on human and ecosystem health: a systematic literature review. Landscape Ecol 2020;35:1725–42. doi:10.1007/s10980-020-01053-1.
[58] Tong KP, Kyba CCM, Heygster G, Kuechly HU, Notholt J, Kolláth Z. Angular distribution of upwelling artificial light in Europe as observed by Suomi–NPP satellite. J Quant Spectrosc Radiat Transf 2020;249:107009. doi:10.1016/j.jqsrt.2020.107009.
[59] United Nations 1979 Convention on long-range transboundary air pollution and its protocols [E/], UN, New York; Geneva: ECE/EBAIR/50; 1996. (Last accessed 7 September 2022) https://digitallibrary.un.org/record/237573?ln=en .
[60] United Nations. Report of the international law commission. Seventieth session (30 April 1 June And 2 July 10 August 2018). General Assembly, Official Records, Seventy Third Session. UN; 2018. p. 171. VI. Protection of the atmosphere. (Last accessed 7 September 2022) https://legal.un.org/ilc/reports/2018/.
[61] Zamorano J, García C, González R, Tapia C, Sánchez de Miguel A, Pascual S, Gallego J, González E, et al. STARS4ALL night sky brightness photometer. Int J Sustain Lighting 2016;35:49–54. doi:10.26607/ijsl.v18i0.21.